Preprints of the 21st IFAC World Congress (Virtual)
Berlin, Germany, July 12-17, 2020

Extremum Seeking Control for Multi-Rotor Wind Turbine in the Full-Load Region

Fabio Spagnolo [**] **Dimitrios Papageorgiou** [*] **Roberto Galeazzi** [*]
Jesper Sandberg Thomsen [**] **Kim Hylling Sørensen** [**]

[*] *Department of Electrical Engineering, Technical University of Denmark, DK-2800 Kgs. Lyngby, Denmark, (e-mail: dimpa,rg@elektro.dtu.dk).*
[**] *Vestas Wind Systems Denmark (e-mail:fasal,KIHSO,jstho@vestas.com)*

Abstract: Multi-rotor wind turbines facilitate higher power production at a lower cost compared to their single-rotor counterparts. However, the larger induced loads due to yaw moments may lead to faster wear and tear on the tower structure and need be appropriately handled by means of pitch control. This paper investigates the feasibility of two different pitch control schemes based on extremum seeking principles for multi-rotor wind turbines in the full-load region. The proposed solutions are tested in simulation. Their performance is compared to that of a benchmark controller with respect to generator speed regulation, power optimisation and fatigue mitigation. The results show that the designed controllers match the performance of the conventional solution at the cost, however, of increased structural stress on the tower.

Keywords: Extremum seeking control, Multi-rotor wind turbine, Control of renewable energy resources, Optimal operation and control of power systems

1. INTRODUCTION

The need for increased wind power production has revealed a challenge with respect to the induced construction cost of larger single-rotor wind turbines (SRT). Higher power ratings imply bigger parts to be installed, with immediate relapse on the cost and complexity of the installation logistics. Moreover, the weight of the rotor increases by the cube of its radius, while the associated power increases by the square. As such, the cost of the rotor production grows faster than the gained power. A possible alternative to larger SRT could be the multi-rotor wind turbine (MRT) because of its lower rotor cost-to-power ratio, since more nacelles can be mounted on the same tower. However, this structure is susceptible to increased stress from load forces and moments, especially in the full-load region, that may lead to higher structural wear. Due to this trade-off, efficient control strategies for power maximisation and fatigue mitigation are highly desirable in the wind power industry.

The MRT control challenge and a possible solution is presented by (Sørensen et al., 2018). The pitch references of four individual gain-scheduling controllers are combined with the signals of two PI regulators, based on tower fore-aft velocity feedback. The additive signals improved tower stiffness, thus mitigating fatigue and enhancing mean power production, in a wide range of operative wind velocities. While the literature about MRT control is scarce, many sources cover power optimization and fatigue mitigation of wind farms and SRT. For instance, (Barradas-Berglind et al., 2014) mitigated both power fluctuations and fatigue on the rotor shaft of an SRT, integrating an online description of fatigue to a model predictive control scheme. Power optimization and fatigue mitigation of wind farms is handled by means of model predictive control, traditional optimal control or even model-free techniques, such as game theory or Extremum Seeking Control (ESC), see e.g. (Kazda et al., 2016) and (Knudsen et al., 2014). The authors in (Ebegbulem and Guay, 2018) applied a gradient-based ESC scheme with adaptive design to power optimization of wind farms. Perturbation-based ESC proved useful to maximize power production of SRT in partial load region, see e.g. (Creaby et al., 2009) and (Ghaffari et al., 2013). Fatigue mitigation was included to the ESC optimization objectives in (Xiao et al., 2016).

This paper addresses the problem of generator speed regulation through ESC pitch control for the MRT in the full load region. Performance is independent of modelling, as ESC does not exploit any knowledge of the MRT dynamics and parameters during operations. Furthermore, no wind speed knowledge is required. Three different ESC schemes are proposed, one exclusively focusing on generator speed regulation and two that also consider fatigue mitigation. The performance of the corresponding closed-loop systems is evaluated in a simulation environment and the proposed control schemes are compared to the solution developed by (Sørensen et al., 2018), referred to as benchmark controller in the remainder of this paper.

The rest of the paper is organized as follows: Section 2 describes the MRT system and formulates the problem at hand. Section 3 details the systematic design of the ESC schemes, while Section 4 presents the results obtained from simulations and compares the ESC solutions to the benchmark controller. Last, Section 5 draws conclusions on the presented work.

2. SYSTEM DESCRIPTION AND OBJECTIVES

2.1 Multi-rotor wind turbine system

The simulation model of the MRT is similar to the Vestas demonstrator shown in Fig. 1, except that the model has higher power ratings. The MRT has four rotors mounted downwind on the same support structure, each rated for 5 MW. Hence the

Fig. 1. Vestas MRT demonstrator, consisting of 4 V29 225 kW nacelles and rotors. Courtesy of Vestas Wind Systems A/S.

MRT can produce up to 20 MW. The turbines operate in the 2 - 20 m/s wind range. Rated wind and generator speeds are 12.4 m/s and 122.9 rad/s, respectively.

The Simulink model of the MRT is provided by (Sørensen et al., 2018) and it includes four National Renewable Energy Laboratory (NREL) 5 MW SRT blocks and a model of the support structure. The model of the SRT has been developed by (Jonkman et al., 2009). The aerodynamic subsystem produces the rotor torque and the thrust force as the combined action of three factors: the relative wind speed relative to the rotor blades V_{rot}, the pitch angle β and the rotor speed Ω_r. The rotor aerodynamics is described by means of two static relations

$$\tau_r = \frac{1}{2} V_{rot}^3 \rho A C_p(\lambda, \beta) \Omega_r^{-1} \tag{1}$$

$$F_t = \frac{1}{2} V_{rot}^2 \rho A C_t(\lambda, \beta) \tag{2}$$

with C_p and C_t being the power and thrust coefficients, respectively. These coefficients are provided as look-up tables functions of the pitch angle and the tip speed ratio $\lambda = \frac{R\Omega_r}{V_{rot}}$. ρ is the air density and A is the rotor disc area.

The rotor speed and the generator speed Ω_g are the outcome of the dynamic torque balance between the rotor side and the generator side of the drive-train. This includes the gearbox with torsional spring constant, viscous friction and a gear ratio. The model is a third order system. The pitch actuator is modeled as a second order system with input delay. A proportional controller compensates for the actuator delay.

The non-linear dynamics of the support structure is presented in (Sørensen et al., 2018). The model does not include gravitational loads, aerodynamic stiffening or damping from rotors. Blades dynamics is not included and the arms are assumed to be very stiff. The inputs to the structure are 4 point thrust forces at the tip of each arm. The linearized equations are utilised to compute the structural moments relevant to fatigue evaluation.

2.2 The benchmark controller

Each SRT implements the variable-speed/variable-pitch, pitch-to-feather control strategy as described by (Bianchi et al., 2006). The SRT controllers receive as inputs the power demand by the network and the generator angular speed. These inputs are used to generate the power set-point to the generator and a pitch set-point to the aerodynamics subsystem. Overall the MRT has four power references and four pitch signals. The benchmark controller feeds additive pitch signals to the baseline set-points of each SRT. The additive signals are computed based on fore-aft tower velocity and displacement feedback and they are shown to be beneficial against fatigue. In particular, the scheme increases the dampening and the stiffness of the support structure (Sørensen et al., 2018).

2.3 Control objectives

The first control objective is to regulate the generator speed to its rated value, while rejecting unknown wind changes and without exploiting any knowledge of the plant model during operations. With all turbines operating in full load region, the second control objective is to keep power output as close as possible to its rated value. The third objective is limitation of structural fatigue. Comparison of the proposed schemes to the benchmark controller, will be carried out based on fulfilment of the control objectives. This study investigates the feasibility of the ESC scheme for this problem, therefore the analysis is restricted to the noise-free case.

3. EXTREMUM SEEKING CONTROL DESIGN

ESC is a dynamic optimization technique that computes the optimal reference set-point that keeps the output of an unknown mapping at the extremum. The cost, i.e. the instantaneous output value, is measurable and it depends on the system dynamics. The correct estimation of the mapping gradient is crucial to compute the optimal reference set-point. Pertubation-based ESC (PESC), as presented by (Ariyur and Krstic, 2003), does not require any knowledge of the system dynamics in doing so. Instead a dithering sinusoidal perturbation is continuously added to the estimated reference set-point. The gradient information is in the amplitude change of the dithering due to propagation into the system. It can be recovered from the measured output through a demodulation sine wave, after removing bias and low frequency components from the signal. The optimal reference set-point is estimated from the gradient information by means of an integral action, which is also useful to reject unknown disturbances. In the following the PESC formulation developed by (Ariyur and Krstic, 2003, Chapter 1) is utilized, because that design allows to handle systems with slow dynamics. This characteristic is particularly useful in the case of the MRT, because the open-loop dynamics of the drive-train is relatively slow compared to the dynamics of the pitch actuator. Furthermore, that design procedure ensures local exponential convergence of the scheme.

3.1 ESC architecture

The proposed ESC architecture includes four identical SISO ESC loops, each comprising three blocks: the local SRT, the measured cost and the ESC. Each loop utilizes information from the local SRT to compute the measured cost. The expression of the measured cost depends on the optimization objectives, and it is based on local information only, i.e. the ESC loops do not share information. Each ESC outputs the pitch reference, which is fed to the local SRT, while the power reference is kept fixed to its nominal value.

3.2 Perturbation-based ESC for Speed Regulation

The block diagram of the adopted SISO ESC loop is shown in Fig. 2. The scheme includes two subsystems, namely the plant and the ESC, where $F_i(s)$ and $F_o(s)$ describe the input

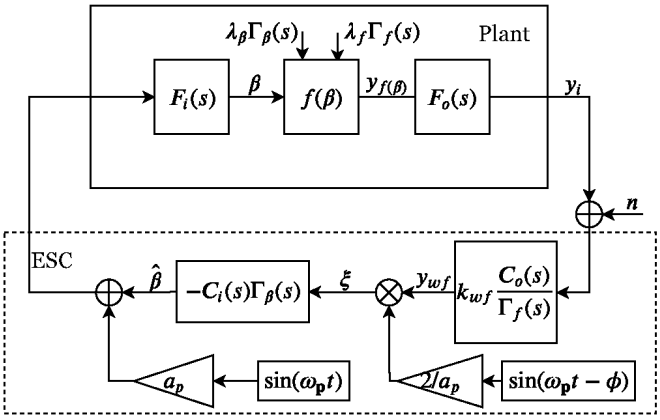

Fig. 2. Block diagram of the adopted SISO ESC loop. Adapted from (Ariyur and Krstic, 2003, Chapter 1)

and output dynamics, respectively. The following assumptions are adopted.

Assumption 1. The input dynamics $F_i(s)$ and output dynamics $F_o(s)$ are BIBO stable and proper transfer functions.

For the MRT system, $F_i(s)$ is the dynamics of the pitch actuator ($F_i(s) = 1/(0.13s+1)$), whereas $F_o(s)$ indicates that a pitch action does not reflect immediately on the generator speed, due to the drive-train. The output dynamics $F_o(s)$ has been estimated through simulations by means of step responses($F_o(s) = 1/(5s+1)$). The mapping $f(\beta)$ is an unknown function of the pitch angle β complying with the following assumption:

Assumption 2. The mapping $f(\beta)$ is $\mathscr{C}^2$ with respect to β. Furthermore the sign of the second derivative f'' evaluated at the optimal pitch β^* is known, and determines whether the extremum is a maximum (negative) or a minimum (positive).

Here the optimization objective is the regulation of the generator speed to its rated value Ω_N. Therefore, the output of the mapping is chosen to be the square of the local generator speed error, as it measures the quality of the generator speed regulation and it has a global minimum in $\Omega_{g,i} = \Omega_N$. Furthermore the function is $\mathscr{C}^2$ with respect to β

$$y_{f(\beta)} = (\Omega_{g,i} - \Omega_N)^2 . \tag{3}$$

The explicit dependence of $y_{f(\beta)}$ on the pitch angle is unknown but (3) fulfils Assumption 2. Therefore it is possible to compute the Taylor approximation of (3) in the neighbourhood of β^*

$$y_{f(\beta)} \approx f(\beta^*) + \frac{f''}{2}(\beta - \beta^*)^2 . \tag{4}$$

The minimum $f(\beta^*) = 0$ indicates zero generator speed error and it is reached when β matches the optimal pitch β^*. Equation (3) has a global minimum, therefore f'' is positive.

According to (Ariyur and Krstic, 2003, Chapter 1), both β^* and $f(\beta^*)$ vary over time. The time variations have known shapes, e.g. step changes, but unknown size, as stated below:

Assumption 3. The Laplace transforms of β^* and $f(\beta^*)$ are

$$\mathscr{L}\{\beta^*\} = \lambda_\beta \cdot \Gamma_\beta(s),\ \mathscr{L}\{f(\beta^*)\} = \lambda_f \cdot \Gamma_f(s) \tag{5}$$

where $\Gamma_\beta(s)$ and $\Gamma_f(s)$ are known, strictly proper and rational transfer functions. They describe the shape of the time variations of β^* and $f(\beta^*)$. Unstable poles of $\Gamma_\beta(s)$ are not zeros of $F_i(s)$. The gains λ_β and λ_f are typically unknown and represent the size of the time variations.

The value β^* depends on the unknown wind speed acting on the rotor, and it continuously changes. In the following, step changes on β^* are assumed. On the other hand $f(\beta^*)$ does not change, as the objective of the first ESC is to regulate the generator speed to Ω_N. Then $y_{f(\beta)}$ is fed to the output dynamics $F_o(s)$. The output of $F_o(s)$ is the squared generator speed error $y_i = (\Omega_{g,i} - \Omega_N)^2$. The goal of the ESC is to achieve local exponential convergence of the output error $\tilde{y} = y_i - f(\beta^*)$ to a neighbourhood of the origin. It is assumed that no measurement noise acts on the measured cost, i.e. $n = 0$.

Within the ESC, the washout filter $WF(s)$ is first applied to y_i

$$WF(s) = k_{wf} C_o(s)/\Gamma_f(s) \tag{6}$$

where k_{wf} is the filter gain and $C_o(s)$ is the output compensator to be designed. $WF(s)$ removes bias and low frequency components from the signal. The output compensator $C_o(s)$ is designed in adherence with the following assumption:

Assumption 4. The following notation is introduced:

$$H_o(s) = k_{wf}\frac{C_o(s)}{\Gamma_f(s)},\ F_o(s) = k_{wf}C_o(s),\ \frac{F_o(s)}{\Gamma_f(s)} = H_{o,sp}H_{o,bp} \tag{7}$$

where $H_{o,sp}(s) = k_{wf}C_o(s)$ is the strictly proper part of $H_o(s)$ and $H_{o,bp}(s) = \frac{F_o(s)}{\Gamma_f(s)}$ is the biproper part of $H_o(s)$. Let a, denote the smallest in absolute value among the real parts of all the poles of $H_{o,sp}(s)$ and let b, denote the largest among the moduli of all the poles of $F_i(s)$ and $H_{o,bp}(s)$. The ratio $M = a/b$ is sufficiently large.

Dithering and demodulation signals operate together to recover missing gradient information. The sine waves in Fig. 2 are completely defined by the perturbation amplitude a_p, the perturbation frequency ω_p and the phase shift ϕ. The recovered gradient information ξ is utilized by the estimation algorithm $EA(s) = -C_i(s)\Gamma_\beta(s)$ to compute the pitch reference $\hat{\beta}$. The input compensator $C_i(s)$ is to be designed such that the following assumption holds:

Assumption 5. The transfer function $H_i(s) \triangleq C_i(s)\Gamma_\theta(s)F_i(s)$ is strictly proper.

If the ESC design complies with the above stated assumptions, then local exponential convergence of the output error can be guaranteed (Ariyur and Krstic, 2003, Theorem 1.8).

Theorem 1. For the system in Fig. 2, under Assumptions 1-5, the output error $\tilde{y}$ achieves local exponential convergence to an $\mathscr{O}(a_p^2 + \delta^2)$ neighbourhood of the origin, where $\delta = 1/\omega_p + 1/M$, provided that $n = 0$ and:

(1) Perturbation frequency ω_p is sufficiently large, and $\pm j\omega_p$ is not a zero of $F_i(s)$.
(2) Unstable zeros of $\Gamma_f(s)$ are also zeros of $C_o(s)$.
(3) Unstable poles of $\Gamma_\theta(s)$ are not zeros of $C_i(s)$.
(4) $C_o(s)$ and $\frac{1}{1+L(s)}$ are BIBO stable where

$$L(s) = \frac{a_p f''}{4}\mathrm{Re}\{e^{j\phi}F_i(j\omega_p)\}H_i(s) \tag{8}$$

The output compensator must fulfil Assumption 4. In the case of strictly proper $F_o(s)$ with a certain number of slow poles compared to the input dynamics, this could be achieved by including as many fast poles to $C_o(s)$ as there are slow poles in $F_o(s)$, see (Ariyur and Krstic, 2003).

The output dynamics $F_o(s)$ has one slow pole compared to the input dynamics $F_i(s)$; hence $C_o(s)$ is designed with one fast pole $p > 0$ that guarantees BIBO stability $C_o(s) = s/(s+p)$. The pole location has been tuned in simulation and the design value is given in Table 1. Conditions (2) and (4) of Theorem 1 are fulfilled.

Following the guidelines provided by (Ariyur and Krstic, 2003, Chapter 1), these design choices have been made: the perturbation amplitude is large enough, such that the sine is visible in the estimated pitch reference, i.e. $a_p = 0.2$; the perturbation frequency is set slightly larger than the frequency of the pole of $F_i(s)$, i.e. $\omega_p = 8.5$ in rad/s; no phase shift is introduced into the demodulation signal.

Last, the estimation algorithm is designed such that it has minimum relative degree, in order to guarantee better phase margins (Ariyur and Krstic, 2003, Chapter 1). A PI regulator is chosen as estimation algorithm $EA(s)$ because it has a relative degree zero, and it allows to fulfill Assumption 5, i.e. $EA(s) = (k_p s + k_i)/s$, where the parameters k_p and k_i have been tuned for each ESC loop in order to fulfil condition (4) of Theorem 1. The resulting tuning parameters are listed in Table 1.

3.3 Fatigue Mitigation: adding a low pass filter

The sinusoidal signals utilized to recover gradient information propagate also on the support structure, with a possible negative impact on fatigue. For instance, the demodulation injects a $\cos(2\omega_p t)$ through the pitch actuators. The cosine signal is a negative side effect of demodulation that fatigue mitigation techniques have to deal with. To achieve this a first order low pass filter is placed between the demodulation and the PI regulator. This technique allows to mitigate the side effect of dithering and demodulation; however convergence may be challenged, as filtering could compromise recovery of the gradient information (Ariyur and Krstic, 2003). The estimation algorithm EA(s) is rewritten as follows:

$$EA(s) = C_i(s)\Gamma_\theta(s) = (k_p s + k_i)/(\tau_{LPF} s^2 + s) \qquad (9)$$

New parameters values are tuned through simulation and listed in Table 1. The remainder of the design is unchanged.

3.4 Fatigue Mitigation: changing the measured cost

Formulating the pitch regulation problem as an extremum seeking control allows some degrees of flexibility in the definition of $y_{f(\beta)}$, and in turn of the measured cost. For instance, the measured cost can be expanded to include a fatigue related term. This is the core of the second fatigue mitigation technique, in which the measured cost is rewritten as

$$y_i = y_{gr,i} + y_{fm,i}, \;\; y_{gr,i} = \frac{W_i}{\sigma^2_{\Omega_g}}(\Omega_{g,i} - \Omega_N)^2 \qquad (10)$$

$$y_{fm,i} = \frac{1 - W_i}{\sigma^2_{F_i}} F_i^2 \quad i = 1, \ldots, 4 \qquad (11)$$

The measured cost consists of two terms, i.e. $y_{gr,i}$ and $y_{fm,i}$. The former deals with the generator speed regulation, while the latter deals with the fatigue mitigation. The weight $W_i \in (0, 1]$ allows trading-off between the two objectives. $y_{gr,i}$ is scaled by the variance of the generator speed, $\sigma^2_{\Omega_g}$. F_i is the description of fatigue at the i-th SRT. $y_{fm,i}$ is also scaled by its variance, $\sigma^2_{F_i}$. This normalization makes the size of $y_{gr,i}$ and $y_{fm,i}$ comparable, which is helpful when tuning W_i.

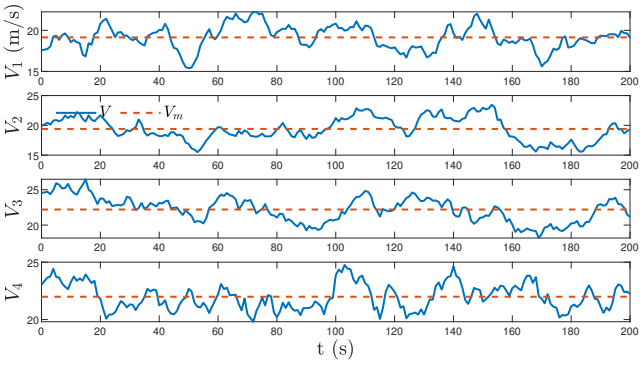

Fig. 3. Benchmark wind scenario, mean wind speed 18 in m/s, normal turbulence.

F_i is chosen to be i-th nacelle fore-aft displacement, as the local information carried by this signal leaves an indirect footprint on structural fatigue. In fact nacelle displacement, does not appear directly in the computation of the moments utilized to evaluate fatigue. However, it is correlated to the tower fore-aft displacement, which is utilized to compute the structural moments. As a matter of facts, reducing the square of each nacelle fore-aft displacement, might be useful to mitigate fatigue.

Tuning of the W_i weights is made considering that the 4 ESC loops are running independently. In principle, the loops might compete against each other to achieve the local optimum – local here refers to the individual nacelle. As a matter of fact, the movement induced on one nacelle by the pitch action to achieve the local trade-off might disturb the action of another ESC loop, especially on the same platform. Since the arms are assumed to be very stiff, the main motion around the vertical axis is platform torsion. This leads to the formulation of two assumptions that are adopted to guide the tuning of the W_i gains.

Assumption 6. Nacelles mounted on the same platform moves in opposite directions with respect to the fore-aft motion.

Under Assumption 6 one ESC per platform compensating for nacelle displacement ($W_i < 1$) is enough to reduce platform torsion and possibly fatigue. The last assumption deal with the structural coupling of nacelles mounted on different platforms.

Assumption 7. The coupling between nacelles mounted on opposite sides of two platforms, is weaker than the coupling between nacelles mounted on the same side of the platforms.

Hence the weights W_i will be lowered one at a time, in nacelles mounted on opposite sides of different platforms.

4. SIMULATION

4.1 Scenarios

Nine test scenarios are provided with the simulation environment that cover the wind speed interval $V_{in} = 4$ in m/s, $V_{out} = 20$ in m/s. Each scenario has 4 different wind profiles, one for each SRT. The shear effect is included in the model, hence top SRTs experience higher average wind speed than bottom ones. The test scenarios are available in the simulation environment and differ each other in average wind speed.

The evaluation of the ESC is carried out in the full load region. The scenario with average wind speed 18 in m/s is utilized for performance assessment as it ensures that the wind speed is never below rated one, especially in the bottom SRTs. If the

wind speed is lower than rated, then the available wind energy is not enough to keep power production at P_N and the ESC would fail to regulate the generator speed. The simulation time is set at 200 s, as stated in (Sørensen et al., 2018). Within the simulation time the average wind speed is above 18 m/s. However, the ESC has to compensate for up to 5 m/s wind speed changes, occurring in less than 20 seconds. The wind scenario is shown in Fig. 3. The parameters shown in Table 1 have been obtained manually in simulation. The tuning parameters refer to each of the three ESC schemes.

4.2 Evaluation criteria

Each ESC scheme is evaluated in terms of generator speed regulation, power production and accumulated structural fatigue. Quality indexes describe the performance of a scheme with respect to the control objectives listed above. The comparison against another scheme is carried out computing the ratios of the indices. In particular, the first ESC is directly compared to the benchmark controller. Instead the two fatigue mitigation techniques are compared against the first ESC, in order to assess the improvement achieved in terms of fatigue mitigation. The quality indexes of each control objective as well as the success criteria are listed in Table 2.

Generator Speed Regulation – The quality of the generator speed regulation at each SRT is measured in terms of mean and variance of the generator speed. If the mean is close to the reference generator speed then the signal oscillates around the reference and the bias is small. A small variance shows the ESC capability to quickly compensate for wind speed variations. Taking the performance of the benchmark controller as a reference, the ESC scheme fulfils the control objective if the ratios of the mean generator speed is almost 1, and the ratios of the generator speed variance are less or equal to 1.

Power Production – The mean power of each SRT when the ESC scheme is operating should at least match the corresponding values obtained with the benchmark controller.

Accumulated Structural Fatigue – Accumulated structural fatigue is measured in terms of damage equivalent loads (DEL), computed through the rainflow counting algorithm (Barradas-Berglind and Wisniewski, 2016). Based on the moments causing structural stress, Sørensen et al. (2018) computed seven DEL, each closely related to a specific structural degree of freedom. The ESC scheme is mitigating fatigue compared to the benchmark controller, when the ratios of the DEL are less or equal to 1.

4.3 Results

The first simulation concerns the ESC designed in Section 3.2. This scheme focuses only on achieving generator speed regulation, with no regards to fatigue mitigation. The ESC has been compared directly to the benchmark controller, and the obtained indexes ratios are reported in Table 3. The first ESC fulfils the targets with respect to generator speed regulation and mean power production. However the accumulated structural fatigue is much more than in the case of the benchmark controller, as witnessed by the DEL ratios being much larger than 1.

A spectral analysis was carried out to identify the motivations of the increased fatigue. The power spectral density (PSD) of the following signals was computed starting from the estimated

Table 1. ESC tuning parameters related to Fig. 3

ESC	Nac	k_p	k_i	p	τ_{LPF}	$\sigma^2_{\Omega_{g,i}}$	$\sigma^2_{u_{y,i}}$
1	1, 2	$[0.6,\ 1.2]\cdot 10^{-3}$	0.05	3			
	3, 4	$[2.5,\ 4]\cdot 10^{-3}$	0.035				
2	1 to 4	$4\cdot 10^{-3}$	0.035	3	0.04		
3	1, 2	1.2	13.5	3		24.6^2	0.75
	3, 4		10.5				10

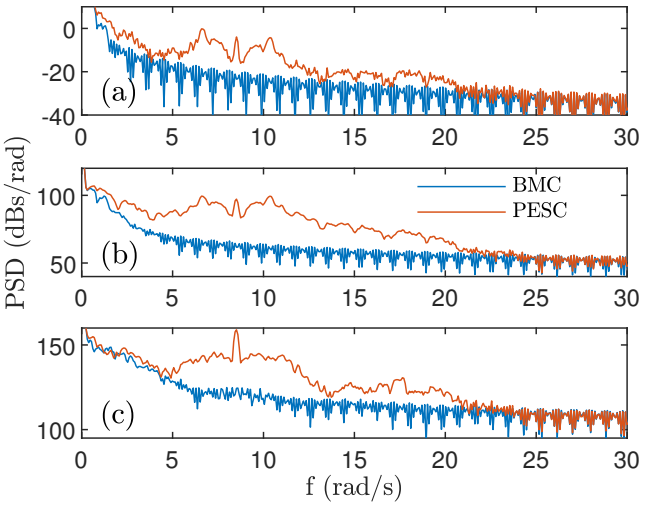

Fig. 4. Benchmark controller (BMC) vs Perturbation-based ESC (PESC). PSD of pitch reference 1 (a), thrust force 1 (b) and tower root moment (c).

pitch angles. Only the power density of the pitch reference 1 is showed due to space limitation. Similar outcomes have been found in the other pitch references. Figure 4 (a) compares the power density of the ESC to that of the benchmark controller. The former has two peaks, respectively in the neighbourhood of 8.5 rad/s and 17.5 rad/s. The first peak is clearly due to the dithering signal, while the second one is a side effect of the demodulation phase. In particular of the $\cos(17.5t)$ term, as explained in Section 3.3.

The excess of power density propagates to the thrust forces, i.e. the inputs of the structural model, as it turns clear in Fig. 4 (b). The excess of power density concentrates in the frequency range where most of the structural mode shapes are. In the neighbourhood of these frequencies, the support structure is not expected to attenuate the extra power density, which then is visible in the moments utilized to compute the DEL. Once again only one PSD is shown, in this case of the Tower Root Moment, see Fig. 4 (c). Similar behaviours have been found in the PSD of the other moments utilized for DEL computation.

The challenge to be addressed by the fatigue mitigation techniques is then to reduce the excess of power density, without compromising convergence of the scheme. In fact, as the power reference is fixed, pitch regulation is expected to be milder. As

Table 2. Quality indices and success criteria.

Objective	Index	Ratio Target	Element(s)
Generator Speed	Mean	≈ 1	SRT 1
	Variance	≤ 1	to 4
Power	Mean	≥ 1	SRT 1 to 4
Fatigue (DEL)	Tower Root Moment Yaw 1 and 2 Moment Arm 1 to 4 Moment	≤ 1	Structure

Table 5. ESC from Section 3.4 vs ESC from Section 3.2. Quality indices ratios

Objective	Index	Ratio
Generator Speed	Mean (SRT 1 to 4)	[1, 1, 1, 1]
	Variance (SRT 1 to 4)	[4.4, 2.5, 2.9, 2.4]
Power	Mean (SRT 1 to 4)	[1, 1, 1, 1]
Fatigue (DEL)	Tower Root Moment	0.90
	Yaw 1 and 2 Moment	[0.63, 0.61]
	Arm 1 to 4 Moment	[0.76, 0.73, 0.84, 0.81]

Table 3. ESC Section 3.2 vs benchmark controller.

Objective	Index	Ratio
Generator Speed	Mean (SRT 1 to 4)	[1, 1, 1, 1]
	Variance (SRT 1 to 4)	[1, 1, 1, 1]
Power	Mean (SRT 1 to 4)	[1, 1, 1, 1]
Fatigue (DEL)	Tower Root Moment	5.75
	Yaw 1 and 2 Moment	[5.35, 4.35]
	Arm 1 to 4 Moment	[4.76, 4.69, 3.64, 3.86]

such the variance of the generator speed is like to increase, mainly because the ESC struggles more to compensate for the unknown wind changes. The fatigue mitigation technique described in Section 3.3 could partially mitigate the excess of power density and with that, reduce the DEL ratios compared to the first ESC. Still the DEL reduction is not enough to obtain comparable fatigue to the benchmark controller. The price to mitigate fatigue is wider generator speed variance. Instead power production remains unchanged, as the power reference is fixed. The quality indexes ratios are listed in Table 4. The table compares the ESC with low pass filter to the ESC for speed regulation.

The second technique investigates the possibility of achieving fatigue mitigation by acting directly on the measured cost, instead of redesigning the estimation algorithm. Tuning of the W_i weights was carried out manually in simulation following Assumptions 6-7. The resulting weights are $W_1 = 0.75$, $W_2 = 1$ while W_3 and $W_4 = 0.8$. Simulations with the wind scenario in Fig.3 reveal that this scheme achieves slightly better fatigue mitigation compared to that one including the low pass filter. In fact it sensibly reduces the generator speed variance, compared to the low pass filter based ESC. However, it is not possible to mimic the fatigue performance achieved by the benchmark controller. Once again power production is not changed, since the power reference is fixed to the nominal value. Quality indexes ratios are shown in Table 5.

5. CONCLUSIONS

Three ESC strategies were proposed for pitch control of a multi-rotor wind turbine in the full load region. A first ESC scheme was implemented that could achieve similar performance to the benchmark controller proposed by Sørensen et al. (2018) in terms of generator speed regulation and mean power production. The increased structural fatigue motivated the exploration of mitigation strategies. Two modified ESC schemes were proposed. The first included a low pass filter, while the second required a new measured cost. Both approaches relieved structural fatigue, without however achieving the performance of the benchmark controller, i.e. the variance of the generator speed was increased. Simulation results showed that ESC is able to achieve the generator speed regulation and mean power production objectives, without any knowledge of the wind speed. However in its present configuration is not suitable

Table 4. ESC from Section 3.3 vs ESC from Section 3.2. Quality indexes ratios.

Objective	Index	Ratio
Generator Speed	Mean (SRT 1 to 4)	[1, 1, 1, 1]
	Variance (SRT 1 to 4)	[5.3, 4.2, 2.5, 3.5]
Power	Mean (SRT 1 to 4)	[1, 1, 1, 1]
Fatigue (DEL)	Tower Root Moment	0.90
	Yaw 1 and 2 Moment	[0.62, 0.63]
	Arm 1 to 4 Moment	[0.79, 0.75, 0.85, 0.84]

for mitigating structure fatigue by direct computation of the pitch references.

REFERENCES

Ariyur, K.B. and Krstic, M. (2003). *Real-Time Optimization by Extremum-Seeking Control*. Wiley.

Barradas-Berglind, J.J. and Wisniewski, R. (2016). Representation of fatigue for wind turbine control. *Wiley Online Library*, 2189 – 2203. doi:10.1002/we.1975.

Barradas-Berglind, J.J., Wisniewski, R., and Soltani, M. (2014). Fatigue damage estimation and data-based control for wind turbines. *IET Control Theory & Applications*, 1042–1050. doi:10.1049/iet-cta.2014.0730.

Bianchi, F.D., De Battista, H., and Mantz, R.J. (2006). *Wind Turbine Control Systems. Principles, Modelling and Gain Scheduling Design*. Springer.

Creaby, J., Li, Y., and Seem, J.E. (2009). Maximizing wind turbine energy capture using multivariable extremum seeking control. *Wind Engineering*, 361 – 388. doi: 10.1260/030952409789685753.

Ebegbulem, J. and Guay, M. (2018). Power maximization of wind farms using discrete-time distributed extremum seeking control. *IFAC*, 339–344. doi:10.1016/j.ifacol.2018.09.323.

Ghaffari, A., Krstic, M., and Seshagiri, S. (2013). Power optimization and control in wind energy conversion systems using extremum seeking. *1st American Control Conference*, 2241 – 2246. doi:10.1109/ACC.2013.6580168.

Jonkman, J., Butterfield, S., Musial, W., and Scott, G. (2009). Definition of a 5-mw reference wind turbine for offshore system development. Technical report, National Renewable Energy Lab.(NREL), Golden, CO (United States).

Kazda, J., Göçmen, T., Giebel, G., Courtney, M., and Cutululis, N. (2016). Framework of multi-objective wind farm controller applicable to real wind farms. *Wind Europe Summit*. URL `https://shorturl.at/eFGKL`.

Knudsen, T., Bak, T., and Svenstrup, M. (2014). Survey of wind farm control—power and fatigue optimization. *Wind Energy*, 1333 – 1351. doi:10.1002/we.1760.

Sørensen, K.H., Knudsen, T., Filsoof, O.T., Hovgaard, T.G., Grunnet, J.D., Neto, J.X.V., Wisniewski, R., et al. (2018). Multi-rotor wind turbine control challenge - a benchmark for advanced control development. *IEEE International Conference on Control Applications*, 1615–1622. doi: 10.1109/CCTA.2018.8511511.

Xiao, Y., Li, Y., and Rotea, M.A. (2016). Multi-objective extremum seeking control for enhancement of wind turbine power capture with load reduction. *Journal of Physics*, 1 – 10. doi:10.1088/1742-6596/753/5/052025.